The Astrophysical Journal, 743:62 (10pp), 2011 December 10 doi:10.1088/0004-637X/743/1/62

VERITAS OBSERVATIONS OF GAMMA-RAY BURSTS DETECTED BY *SWIFT*

V. A. Acciari[1], E. Aliu[2], T. Arlen[3], T. Aune[4,28], M. Beilicke[5], W. Benbow[1], S. M. Bradbury[6], J. H. Buckley[5], V. Bugaev[5], K. Byrum[7], A. Cannon[8], A. Cesarini[9], J. L. Christiansen[10], L. Ciupik[11], E. Collins-Hughes[8], M. P. Connolly[9], W. Cui[12], C. Duke[13], M. Errando[2], A. Falcone[14], J. P. Finley[12], G. Finnegan[15], L. Fortson[16], A. Furniss[4], N. Galante[1], D. Gall[12], S. Godambe[15], S. Griffin[17], J. Grube[11], R. Guenette[17], G. Gyuk[11], D. Hanna[17], J. Holder[18], G. Hughes[19], C. M. Hui[15], T. B. Humensky[20], D. J. Jackson[10], P. Kaaret[21], N. Karlsson[16], M. Kertzman[22], D. Kieda[15], H. Krawczynski[5], F. Krennrich[23], M. J. Lang[9], A. S. Madhavan[23], G. Maier[19], S. McArthur[5], A. McCann[17], P. Moriarty[24], M. D. Newbold[15], R. A. Ong[3], M. Orr[23], A. N. Otte[4], N. Park[20], J. S. Perkins[1], M. Pohl[19,25], H. Prokoph[19], J. Quinn[8], K. Ragan[17], L. C. Reyes[20], P. T. Reynolds[26], E. Roache[1], H. J. Rose[6], J. Ruppel[25], D. B. Saxon[18], M. Schroedter[23], G. H. Sembroski[12], G. D. Şentürk[27], A. W. Smith[7], D. Staszak[17], S. P. Swordy[29], G. Tešić[17], M. Theiling[1], S. Thibadeau[5], K. Tsurusaki[21], A. Varlotta[12], V. V. Vassiliev[3], S. Vincent[15], M. Vivier[18], S. P. Wakely[20], J. E. Ward[8], T. C. Weekes[1], A. Weinstein[3], T. Weisgarber[20], D. A. Williams[4], and M. Wood[3]

[1] Fred Lawrence Whipple Observatory, Harvard-Smithsonian Center for Astrophysics, Amado, AZ 85645, USA
[2] Department of Physics and Astronomy, Barnard College, Columbia University, NY 10027, USA
[3] Department of Physics and Astronomy, University of California, Los Angeles, CA 90095, USA
[4] Santa Cruz Institute for Particle Physics and Department of Physics, University of California, Santa Cruz, CA 95064, USA
[5] Department of Physics, Washington University, St. Louis, MO 63130, USA
[6] School of Physics and Astronomy, University of Leeds, Leeds, LS2 9JT, UK
[7] Argonne National Laboratory, 9700 S. Cass Avenue, Argonne, IL 60439, USA
[8] School of Physics, University College Dublin, Belfield, Dublin 4, Ireland
[9] School of Physics, National University of Ireland Galway, University Road, Galway, Ireland
[10] Physics Department, California Polytechnic State University, San Luis Obispo, CA 94307, USA
[11] Astronomy Department, Adler Planetarium and Astronomy Museum, Chicago, IL 60605, USA
[12] Department of Physics, Purdue University, West Lafayette, IN 47907, USA
[13] Department of Physics, Grinnell College, Grinnell, IA 50112-1690, USA
[14] Department of Astronomy and Astrophysics, 525 Davey Lab, Pennsylvania State University, University Park, PA 16802, USA
[15] Department of Physics and Astronomy, University of Utah, Salt Lake City, UT 84112, USA
[16] School of Physics and Astronomy, University of Minnesota, Minneapolis, MN 55455, USA
[17] Physics Department, McGill University, Montreal, QC H3A 2T8, Canada
[18] Department of Physics and Astronomy and the Bartol Research Institute, University of Delaware, Newark, DE 19716, USA
[19] DESY, Platanenallee 6, 15738 Zeuthen, Germany
[20] Enrico Fermi Institute, University of Chicago, Chicago, IL 60637, USA
[21] Department of Physics and Astronomy, University of Iowa, Van Allen Hall, Iowa City, IA 52242, USA
[22] Department of Physics and Astronomy, DePauw University, Greencastle, IN 46135-0037, USA
[23] Department of Physics and Astronomy, Iowa State University, Ames, IA 50011, USA
[24] Department of Life and Physical Sciences, Galway-Mayo Institute of Technology, Dublin Road, Galway, Ireland
[25] Institut für Physik und Astronomie, Universität Potsdam, 14476 Potsdam-Golm, Germany
[26] Department of Applied Physics and Instrumentation, Cork Institute of Technology, Bishopstown, Cork, Ireland
[27] Columbia Astrophysics Laboratory, Columbia University, New York, NY 10027, USA
Received 2011 April 15; accepted 2011 August 30; published 2011 November 22

ABSTRACT

We present the results of 16 *Swift*-triggered Gamma-ray burst (GRB) follow-up observations taken with the Very Energetic Radiation Imaging Telescope Array System (VERITAS) telescope array from 2007 January to 2009 June. The median energy threshold and response time of these observations were 260 GeV and 320 s, respectively. Observations had an average duration of 90 minutes. Each burst is analyzed independently in two modes: over the whole duration of the observations and again over a shorter timescale determined by the maximum VERITAS sensitivity to a burst with a $t^{-1.5}$ time profile. This temporal model is characteristic of GRB afterglows with high-energy, long-lived emission that have been detected by the Large Area Telescope on board the *Fermi* satellite. No significant very high energy (VHE) gamma-ray emission was detected and upper limits above the VERITAS threshold energy are calculated. The VERITAS upper limits are corrected for gamma-ray extinction by the extragalactic background light and interpreted in the context of the keV emission detected by *Swift*. For some bursts the VHE emission must have less power than the keV emission, placing constraints on inverse Compton models of VHE emission.

Key words: astroparticle physics – gamma-ray burst: general

1. INTRODUCTION

Gamma-ray bursts (GRBs) have been an active area of study since their discovery in the late 1960s (Klebesadel et al. 1973). Observations of GRBs and their afterglows over the last decade are generally consistent with the relativistic fireball framework (e.g., Piran 1999). In this theoretical framework, prompt gamma-ray emission is produced by internal shocks created by relativistic jets with varied Lorentz factors that originate from a central engine. The afterglow emission arises from external shocks set up when outflowing material interacts

[28] Author to whom correspondence may be addressed.
[29] Deceased.

with the surrounding environment. Within this basic fireball framework there have been a number of theories proposed that predict very high energy (VHE) photon production. A proposed physical mechanism that produces VHE radiation in GRBs is inverse Compton (IC) scattering. By this mechanism electrons accelerated by the burst's central engine upscatter relatively soft photons from an external photon field (external inverse Compton; Beloborodov 2005; Wang et al. 2006) or from a photon field generated by synchrotron emission from the electrons themselves (synchrotron self-Compton, SSC; Zhang & Mészáros 2001; Wang et al. 2001).

External shocks may also produce VHE photons. If this is the case, measurements of the spectrum above 10 GeV can directly constrain the medium density as well as the equipartition fraction of the magnetic field (Pe'er & Waxman 2005) in the burst environment. VHE emission delayed by $\sim$100 to $>$10,000 s can be produced by the external forward shock (Meszaros & Rees 1994; Dermer et al. 2000; Fan et al. 2008). GeV emission from electron synchrotron processes in the forward shock has been predicted to be relatively bright (Zou et al. 2009) and it has been proposed (Kumar & Barniol Duran 2009) that such emission was detected by the Large Area Telescope (LAT) on the *Fermi* satellite (Atwood et al. 2009) in the bright gamma-ray burst GRB 080916C (Abdo et al. 2009c). In addition to the GeV synchrotron component, there may also be SSC processes producing VHE photons in the forward shock (Panaitescu 2008). This component is predicted to be less intense than the synchrotron component and therefore difficult to detect with the *Fermi*-LAT, but the very high energies and relatively late emission times (up to several hours) make these photons prime candidates for detection by ground-based, imaging atmospheric Cherenkov telescope (IACT) systems (Zou et al. 2009; Xue et al. 2009).

Yet another possible mechanism for generating delayed VHE photons from GRBs is IC scattering of photons from X-ray flares. The X-Ray Telescope (XRT) on board *Swift* has made it possible to take detailed X-ray observations of fading GRB afterglows on a regular basis. In roughly half of these observations, X-ray flare activity has been observed that takes place hundreds to thousands of seconds after the initial gamma-ray signal (Chincarini et al. 2007). It is predicted that VHE photons could arise from the X-ray photons, produced by late-time central engine activity, interacting with electrons accelerated at the forward shock. It is also possible that the X-ray flares are produced by the forward shock itself and that VHE photons are consequently created through the SSC process. Simultaneous observations of X-ray and VHE afterglows can distinguish between these two possibilities and can constrain the microphysics in the shocks themselves (Wang et al. 2006). While not expected to be a routine event, detection of VHE emission from X-ray flares in GRBs by current-generation IACTs (VERITAS, MAGIC, HESS) should be possible under favorable conditions (Fan et al. 2008; Galli & Piro 2008). Recently, the *Fermi*-LAT detected hard-spectrum ($\Gamma = 1.4$) high-energy emission associated with late-time X-ray flaring activity in GRB 100728A (Abdo et al. 2011). Finally, GRBs have been advanced as a possible class of sources that generate ultra-high-energy cosmic rays (Waxman 2004; Murase et al. 2008; Dermer 2007). In hadronic or combined leptonic/hadronic models, VHE gamma rays are produced by the energetic leptons that are created from cascades initiated by photopion production (Bottcher & Dermer 1998).

There have been several attempts to observe VHE photon emission from GRBs using ground-based facilities but, to date, no conclusive detections have been made. A possible detection of VHE gamma rays associated with the BATSE-detected GRB 970417A was reported (Atkins et al. 2000) by the Milagrito Collaboration but no redshift was determined and no other follow-up observations were made. Even though detection of VHE afterglow emission with IACTs is predicted to be possible, observations by both previous- (Connaughton et al. 1997) and current-generation (Aharonian et al. 2009; Albert et al. 2007) observatories have yielded no significant detections.

Presented here are the results from GRB observations made during an 18 month interval with the Very Energetic Radiation Imaging Telescope Array System (VERITAS) between autumn 2007 and spring 2009. The sample is limited to well-localized bursts observed with at least three of the four VERITAS telescopes.

2. THE VERITAS ARRAY

VERITAS is an array of four IACTs, each 12 m in diameter, located 1268 m a.s.l. at the Fred Lawrence Whipple Observatory in southern Arizona, USA (31°40′30″ N, 110°57′07″ W). The first telescope was completed in the spring of 2005 and the full, four-telescope array began routine observations in the autumn of 2007. The first telescope was installed at a temporary location as a prototype instrument and in the summer of 2009 it was moved to a new location in the array to make the distance between telescopes more uniform and consequently improve the sensitivity of the system (Perkins et al. 2009). The observations presented here were taken with the old array configuration with at least three telescopes in the array operational. Each of the telescopes is of Davies-Cotton design and is equipped with an imaging camera consisting of 499 photomultiplier tubes (PMTs) at the focus, 12 m from the center of the reflector. The angular spacing of the PMTs is approximately 0.°15 resulting in a field of view (FOV) of 3.°5 in diameter. Each PMT has a Winston cone mounted in front of the cathode to reduce the dead space between pixels and to increase the light collection efficiency.

The VERITAS array uses a three-level trigger system that greatly reduces the number of background events. The first level of the trigger system is at the pixel, i.e., PMT, level where the signal from each PMT is fed to a programmable constant fraction discriminator with a threshold of 4–5 photoelectrons. The second trigger level, the camera/telescope trigger, consists of a pattern trigger that requires at least three adjacent pixels satisfying the first level trigger within a $\sim$7 ns coincidence window. Finally, an array-level trigger is satisfied if at least two of the four telescopes in the array are triggered within 100 ns of one another, after correcting for time-of-flight differences. Once the array is triggered, the signals, which are continuously digitized for each PMT using 500 mega-samples per second flash analog to digital converters (FADCs), are read out and stored to disk. The array has an effective area of $\sim 10^3$ m^2 to $\sim 10^5$ m^2 and an energy resolution of 15%–20% over the 100 GeV–30 TeV energy range. The single event angular resolution (68% containment) is better than 0.°14. A more comprehensive description of the VERITAS array can be found in Holder et al. (2006).

3. GAMMA-RAY BURST OBSERVATIONS

GRB observations take priority over all others in the VERITAS observing plan. To facilitate rapid follow-up observations of GRBs detected by satellites, VERITAS control computers are set to receive notices from the GRB Coordinates Network (GCN)[30] over a socket connection through the TCP/IP

[30] http://gcn.gsfc.nasa.gov

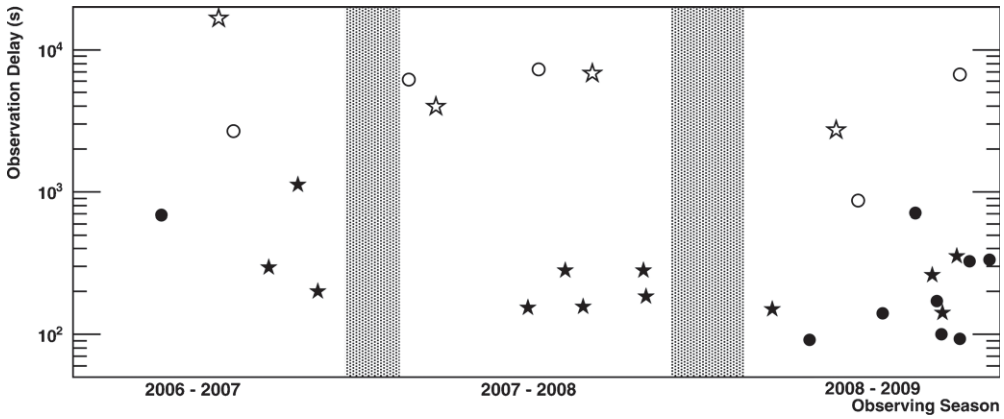

Figure 1. Delay from the start of the burst to the beginning of VERITAS observations for all GRBs with VERITAS data. The open symbols correspond to observations that were delayed due to constraints such as the burst occurring during daylight or below the horizon. Filled symbols are unconstrained observation delays and are primarily determined by the time it takes the telescopes to slew to the burst. The 16 stars correspond to the GRBs discussed in this paper. The shaded regions indicate the annual shutdown of the array due to the summer monsoons.

protocol. Once the GCN notice is parsed by the control computer, an audible alarm notifies the observers on duty that a GRB has occurred. The coordinates of the burst are loaded into the telescope tracking software and the observers are notified to stop current observations and to begin slewing the telescopes to the GRB position, subject to observational constraints such as the Moon and horizon. Currently, the telescopes are capable of simultaneously slewing at a rate of $1^\circ\ s^{-1}$ in both elevation and azimuth. Figure 1 shows the observation delays for all GRBs with VERITAS data over a three-year period. The delay between the satellite trigger and the beginning of GRB observations is usually less than 300 s if the burst is immediately observable, and in several cases this delay is less than 100 s. The dominant contribution to the observation delay is the time it takes the telescopes to slew to the source position.

If the GRB is sufficiently well-localized, as is the case with the bursts presented here, VERITAS observations continue for up to 3 hr after the GRB satellite trigger, again subject to observing constraints. The transition from the prompt to the afterglow phase of a GRB, which can occur hundreds to thousands of seconds after the initial burst, is often accompanied by X-ray flares (Falcone et al. 2007). These flares can be very bright and may be associated with extended activity from the GRB central engine (Burrows et al. 2005) or be from delayed external shocks that could produce a relatively large flux of gamma rays in the ∼100 GeV energy range. For GRBs, the VERITAS strategy of rapid follow-up observations that continue for several hours allows for good temporal coverage of X-ray flare phenomena. Even in the absence of flare activity, it is suggested that a significant flux of high-energy photons from IC processes associated with the GRB afterglow may extend to more than 10 ks after the beginning of the GRB prompt emission (Galli & Piro 2008) and so an observation window of several hours is warranted.

During the period beginning 2007 January and ending 2009 June, VERITAS took follow-up observations of 29 GRBs. Nine of these bursts were detected only by the Gamma-ray Burst Monitor (GBM) on board the *Fermi* satellite and the errors on the localizations were larger than the VERITAS FOV. Analysis of these bursts will be presented in a future publication. The remaining sample of 20 well-localized bursts (19 detected by the *Swift* satellite and 1 by the *INTEGRAL* spacecraft) is reduced to 16 after applying cuts on the hardware status of the array and on the burst elevation (minimum elevation for GRB observations considered in this analysis is 30°). Table 1 lists the general properties of these 16 bursts. The VERITAS observations of GRBs presented here took place during good weather and under dark skies or low-moonlight conditions.

The data were collected in runs with nominal durations of 20 minutes with roughly 30 s of dead time between runs. At the beginning of each run the best source localization to arrive via the GCN socket connection is used as the target for the duration of that run. Twelve of the bursts were observed in "wobble mode" in which the source is displaced some angular distance away from the center of the camera, allowing simultaneous observation and background estimation (Berge et al. 2007). For the GRB observations presented here, the wobble offset was $0.^\circ5$. In the cases of GRB 070419A, GRB 070521, GRB 070612B, and GRB 080604, observations were taken in a tracking mode in which the source is placed at the center of the camera. Historically, GRB observations were taken in tracking mode but wobble mode is now the default method of observation with VERITAS and all GRB observations are currently taken in this fashion. The use of the tracking mode does offer a marginal increase in "raw" sensitivity over the wobble mode but with a significant increase in the uncertainty of the background.

4. DATA ANALYSIS

The data taken on the 16 GRBs were analyzed using the standard VERITAS analysis suite (Cogan et al. 2008). The charge in each FADC trace is determined by summing the samples over an appropriately placed 14 ns wide integration window. The integrated signal from each pixel in the camera results in an image of the air shower at the camera plane. The shower image is cleaned by eliminating any pixel with a signal of less than five standard deviations above its pedestal value, that is, a signal less than five times the standard deviation from the average FADC measurement when no Cherenkov signal is present. Any pixel that registers a signal of at least two and a half standard deviations above its pedestal is also retained provided it is adjacent to at least one of the pixels that exceeds five standard deviations. The cleaned images are then parameterized using the Hillas moment analysis (Hillas 1985). Before performing a full event reconstruction, images with less than five pixels surviving the image cleaning or with an image centroid more than $1.^\circ43$ from the camera center are removed from the analysis. A cut on the integrated charge in each image is made at

Table 1
Details of 16 GRBs Observed by VERITAS

GRB	*Swift* Trigger	T_{90}(s)[a]	Fluence (10^{-7}erg cm^{-2})[b]	T_{trig}[c]	R.A.	Decl.	Error	z
070223	261664	89	17	01:15:00	$10^h13^m48\overset{s}{.}39$	$+43°08'00\overset{''}{.}70$	$0\overset{''}{.}30$	...
070419A	276205	116	5.6	09:59:26	$12^h10^m58\overset{s}{.}83$	$+39°55'34\overset{''}{.}06$	$0\overset{''}{.}15$	0.97[1]
070521	279935	37.9	80	06:51:10	$16^h10^m38\overset{s}{.}59$	$+30°15'21\overset{''}{.}96$	$1\overset{''}{.}70$	0.553?[2]
070612B	282073	13.5	17	06:21:17	$17^h26^m54\overset{s}{.}49$	$-08°45'06\overset{''}{.}3$	$4\overset{''}{.}0$	...
071020	294835	4.2	23	07:02:26	$07^h58^m39\overset{s}{.}78$	$+32°51'40\overset{''}{.}4$	$0\overset{''}{.}250$	2.145[3]
080129	301981	48	8.9	06:06:45	$07^h01^m08\overset{s}{.}20$	$-07°50'46\overset{''}{.}3$	$0\overset{''}{.}3$	...
080310	305288	365	23	08:37:58	$14^h40^m13\overset{s}{.}80$	$-00°10'29\overset{''}{.}60$	$0\overset{''}{.}6$	2.43[4]
080330	308041	61	3.4	03:41:16	$11^h17^m04\overset{s}{.}50$	$+30°37'23\overset{''}{.}53$	$0\overset{''}{.}7$	1.51[5]
080409	308812	20.2	6.1	01:22:57	$05^h37^m19\overset{s}{.}14$	$+05°05'05\overset{''}{.}4$	$2\overset{''}{.}0$	...
080604	313116	82	8.0	07:27:01	$15^h47^m51\overset{s}{.}70$	$+20°33'28\overset{''}{.}1$	$0\overset{''}{.}5$	1.416[6]
080607	313417	79	240	06:07:27	$12^h59^m47\overset{s}{.}24$	$+15°55'08\overset{''}{.}74$	$0\overset{''}{.}5$	3.036[7]
081024A	332516	1.8	1.2	05:54:21	$01^h51^m29\overset{s}{.}71$	$+61°19'53\overset{''}{.}04$	$1\overset{''}{.}9$	...
090102	338895	27	68	02:55:45	$08^h32^m58\overset{s}{.}54$	$+33°06'51\overset{''}{.}10$	$0\overset{''}{.}5$	1.55[8]
090418A	349510	56	46	11:07:40	$17^h57^m15\overset{s}{.}17$	$+33°24'21\overset{''}{.}1$	$0\overset{''}{.}5$	1.6089
090429B	350854	5.5	3.1	05:30:03	$14^h02^m40\overset{s}{.}10$	$+32°10'14\overset{''}{.}6$	$1\overset{''}{.}8$	...
090515	352108	0.036	0.04	04:45:09	$10^h56^m36\overset{s}{.}11$	$+14°26'30\overset{''}{.}3$	$2\overset{''}{.}7$	...

Notes. All information was taken from GCN circulars (http://gcn.gsfc.nasa.gov/gcn3_archive.html).
[a] Duration over which 90% of the emission in the 15–350 keV energy band occurs, as measured by the *Swift*-Burst Alert Telescope (BAT).
[b] 15–150 keV fluence, as measured by the *Swift*-BAT.
[c] UT time of the GRB trigger determined by the *Swift*-BAT.
References. (1) Cenko et al. 2007; (2) Hattori et al. 2007; (3) Jakobsson et al. 2007; (4) Prochaska et al. 2008a; (5) Malesani et al. 2008; (6) Wiersema et al. 2008; (7) Prochaska et al. 2008b; (8) de Ugarte Postigo et al. 2009; (9) Chornock et al. 2009.

$\sim$75 ($\sim$38) photoelectrons for the standard-source (soft-source) analysis. For GRBs, the standard-source analysis is optimized for a weak Crab-like source (3% Crab flux with a spectral index, $\Gamma = 2.5$), while the soft-source analysis gives a reduced energy threshold and assumes a $\Gamma = 3.5$ spectrum. While the spectral characteristics of GRBs are unknown at the highest energies, the standard analysis spectral index of 2.5 was selected based on the average high-energy spectral index, β observed by BATSE (Kaneko et al. 2006). Since it is expected that the extragalactic background light (EBL) will significantly soften the intrinsic GRB spectrum, the soft-source analysis was optimized to the softer assumed spectral index of 3.5. It should be noted that although the analysis is optimized for a specific spectral index and source intensity, this does not preclude the detection of sources with characteristics significantly different than those assumed.

At this stage, any event with images in fewer than two telescopes is rejected because stereo reconstruction is not possible. Furthermore, any event with images in only the two telescopes with the smallest separation is removed as the proximity of these two telescopes ($\sim$35 m) in the old array configuration produced less reliable event reconstruction and an increased background rate that resulted in decreased sensitivity. After event reconstruction, the rejection of background events, which are due largely to cosmic rays, is accomplished by comparing the length and width parameters of shower images with those predicted by Monte Carlo simulations of gamma-ray-initiated air showers (Krawczynski et al. 2006). Finally, a cut on the arrival direction of the gamma ray of $\theta < 0\overset{\circ}{.}13$ ($\theta < 0\overset{\circ}{.}14$) for the standard (soft) analysis is applied, where θ is the angular distance in the FOV from the reconstructed arrival direction of the event to the putative source location. For all bursts presented here, the uncertainty in the GRB position (in all cases $<4''$) is negligible compared to the angular distance cut on arrival direction.

Twelve of the sixteen bursts were observed in wobble mode and the estimation of the background in the signal region is made using the reflected region technique (Aharonian et al. 2001). In the cases of GRB 070419A, GRB 070521, GRB 070612B, and GRB 080604, the observations were made with the GRB positions at the center of the fields of view of the telescopes and a reflected region background estimation is not possible. For these observations the ring-background estimation method (Berge et al. 2007) is employed instead. The significance of the gamma-ray excess in the signal region is then computed using Equation (17) in Li & Ma (1983).

If there is no significant gamma-ray excess detected (i.e., the excess in the signal region is less than five standard deviations above the background region), the 99% confidence level upper limit on the number of signal photons is calculated using the frequentist method of Rolke et al. (2005). From this number, the corresponding upper limit on the integral photon flux above the threshold energy is computed. The energy threshold is defined as the energy at which the product of the detector effective area and assumed source spectrum is maximized. The effective area, and consequently the threshold energy, of VERITAS is strongly dependent on the elevation of the source being observed. As the elevation of the observation decreases, the column density of the atmosphere increases. This results in a gamma ray of some given energy producing a lower Cherenkov photon density at ground level, which increases the energy threshold of detection. However, because the effective area of the instrument is non-zero below the threshold energy defined in this way, gamma rays in this energy range are detectable. For all of the VERITAS data analyzed, a secondary analysis was done using an independent software package and the results obtained are compatible with those presented here.

A search for VHE emission is performed over the entire duration of the VERITAS observations as well as over a shorter timescale that optimizes the sensitivity of VERITAS to a source with a flux that decays as a power law in time. The *Fermi*-LAT has detected more than a dozen GRBs with emission above 100 MeV. This high-energy emission is seen to persist

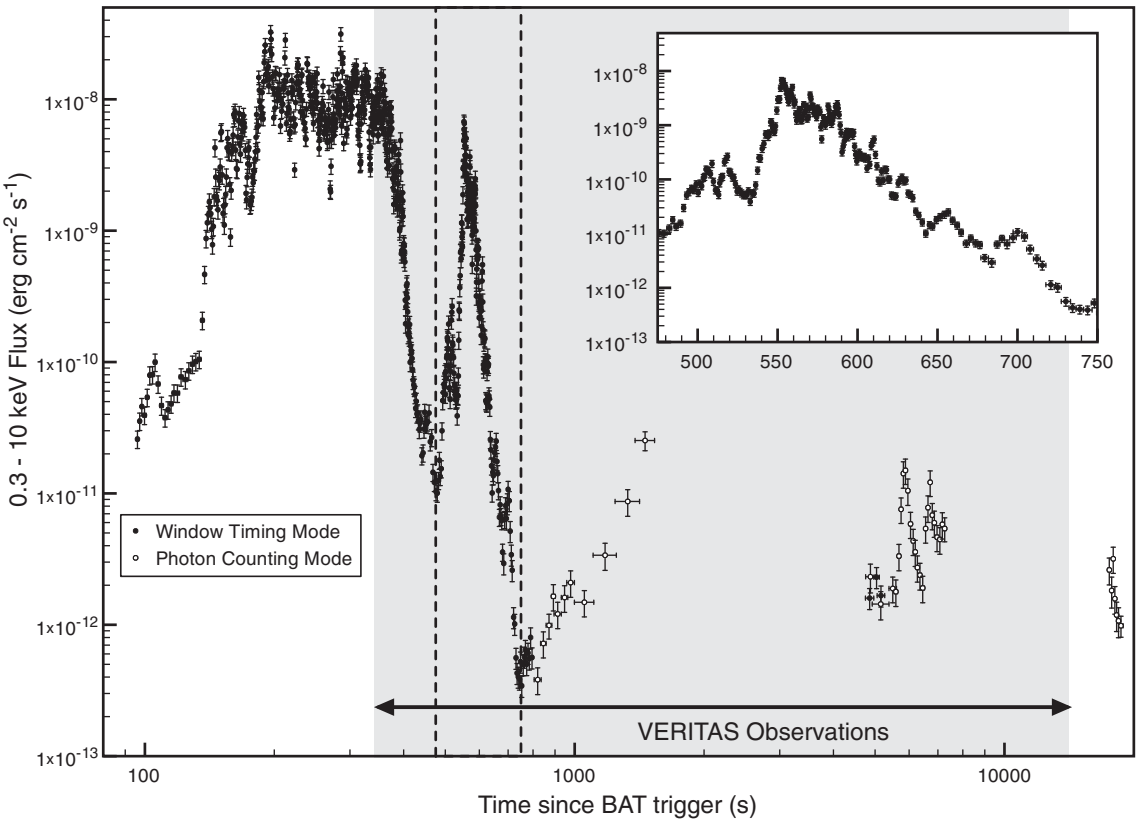

Figure 2. VERITAS observation window of GRB 080310 superimposed on the *Swift*-XRT light curve (Evans et al. 2007, 2009). The inset shows the structure of the X-ray flare (dashed lines) and is the time window over which the search for VHE emission was performed. No significant excess of VHE gamma rays coincident with the X-ray flare (475 s $< t - T_{\rm trig} <$ 750 s) was found.

after the flux in the GBM band has ceased and shows weak spectral evolution with a spectral index between the α and β indices of the Band function fit to the GBM data (Ghisellini et al. 2010). The temporal behavior of the brightest four *Fermi*-LAT-detected bursts, GRB 080916C (Abdo et al. 2009c), GRB 090510 (Pasquale et al. 2010), GRB 090902B (Abdo et al. 2009b), and GRB 090926A (Ackermann et al. 2011), shows a common $\frac{dN}{dE} \sim t^{-\Delta}$ decay, where $1.2 < \Delta < 1.7$ in the observer frame. If it is assumed that the temporal and spectral characteristics of a GRB detected by the *Fermi*-LAT extend to the VHE energy range, the observed power-law temporal decay of the high-energy emission consequently defines an optimal duration over which the search for VHE emission is maximally sensitive. This optimal duration is determined solely by the high-energy temporal power-law index of the GRB, the delay from the GRB trigger time ($T_{\rm trig}$) to the beginning of VERITAS GRB observations, and by, to a lesser extent, the observational backgrounds. For a VERITAS observation beginning 100 s after the GRB $T_{\rm trig}$, the observation window that gives maximum sensitivity is ∼2–5 minutes for GRBs similar to the brightest LAT-detected bursts. For bursts with unknown high-energy behavior, the determination of an optimal time window for VHE observations is not straightforward. However, the maximum sensitivity of a VHE instrument such as VERITAS to a GRB with a power-law decay in time is likely to be on the order of a few minutes.

In the case of GRB 080310, the *Swift*-XRT detected a large X-ray flare beginning ∼475 s after the beginning of the burst as measured by the *Swift*-BAT. VERITAS was on target 342 s after $T_{\rm trig}$ for this burst and observed throughout the X-ray flare. Figure 2 shows the VERITAS observing window for this burst relative to the XRT light curve (Evans et al. 2007, 2009). A search for VHE emission is made coincident with the X-ray flare.

5. RESULTS

An analysis of VERITAS data associated with the 16 GRB positions listed in Table 1 shows no significant excess of VHE gamma-ray events for any GRB over the entire duration of VERITAS observations. Table 2 summarizes the details and results of the VERITAS GRB observations for the sample of GRBs described in Table 1. The significance distributions for both the standard- and soft-source analyses are shown in Figure 3. The sensitivity of the VERITAS array, and the small observation delays with respect to the GRB $T_{\rm trig}$ (half of the burst observations had delays of less than 5 minutes) combine to give some of the most constraining limits on VHE gamma-ray emission from GRB afterglows.

The VHE photon fluxes from objects at cosmological distances are attenuated due to photon absorption by the EBL. Of the sixteen bursts for which results are presented here, nine had redshifts determined by optical follow-up observations. For these bursts, a limit on the intrinsic photon flux of the GRB can be set if one assumes a model of the EBL. For all calculations requiring a model of the EBL, we use the model described in Gilmore et al. (2009). To determine the factor by which the upper limits in Table 2 increase due to effects of the EBL, one must calculate the effective attenuation of VHE photons over the VERITAS waveband, taking into account the spectral response of the instrument. For each GRB observation, the

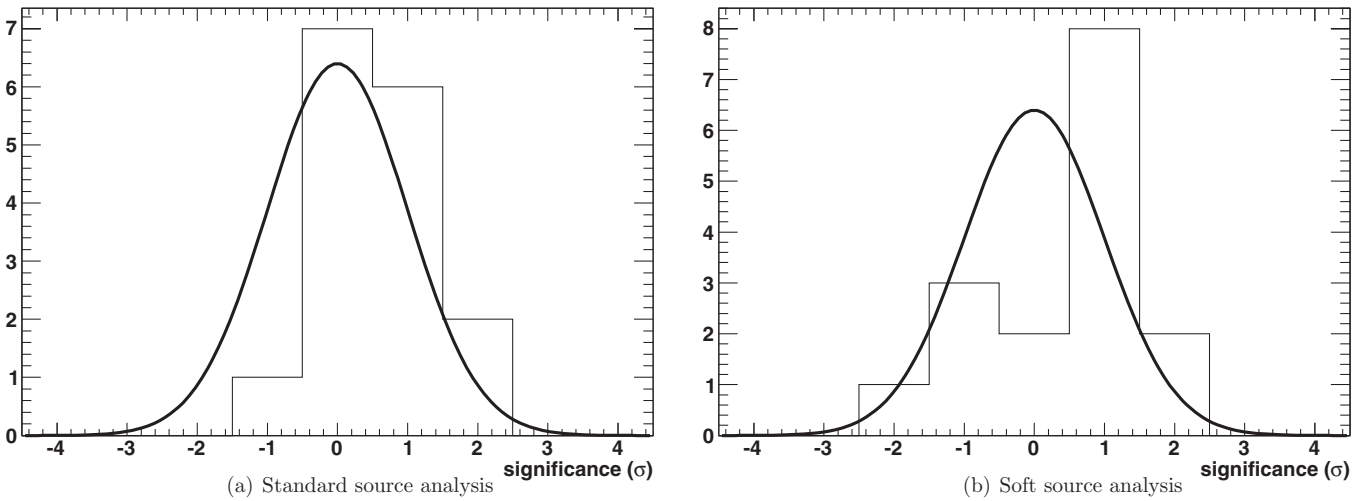

(a) Standard source analysis (b) Soft source analysis

Figure 3. Significance histograms of the 16 GRBs in this sample for both standard- and soft-source analyses. Included in the figures is the normalized Gaussian distribution of mean zero and variance one that the significance histograms should follow if no signal is present. The GRB significances are consistent with having been drawn from the aforementioned Gaussian distribution.

Table 2
VERITAS Observations of Gamma-Ray Bursts

GRB			Elev. Range (°)[c]	Standard-source Analysis			Soft-source Analysis		
	$T_{\rm delay}$ (s)[a]	$T_{\rm obs}$ (min)[b]		$E_{\rm th}$ (GeV)[d]	σ[e]	Upper Limit	$E_{\rm th}$ (GeV)[d]	σ[e]	Upper Limit
070223	1.7×10^4	74.1	67–78	220	1.3	9.5×10^{-12}	150	0.8	2.0×10^{-11}
070419A	295	37.7	32–36	610	−0.1	8.1×10^{-12}	420	−1.0	1.0×10^{-11}
070521	1118	75.4	63–88	190	0.1	4.6×10^{-12}	120	−0.3	9.6×10^{-11}
070612B	201	131.9	46–50	380	0.6	2.5×10^{-12}	230	0.6	7.1×10^{-12}
071020	5259	73.5	30–43	570	1.8	1.7×10^{-11}	330	0.5	2.6×10^{-11}
080129	1456	31.4	47–50	370	1.2	7.7×10^{-12}	220	1.4	1.2×10^{-11}
080310	342	198.0	48–58	270	0.2	2.2×10^{-12}	170	1.8	7.3×10^{-12}
080330	156	107.8	64–88	180	0.2	4.0×10^{-12}	120	−0.7	6.3×10^{-12}
080409	6829	19.0	31–35	1300	0.1	5.3×10^{-11}	720	−0.7	3.8×10^{-11}
080604	281	151.8	33–70	250	1.1	4.7×10^{-12}	160	0.9	1.2×10^{-11}
080607	184	56.0	32–46	400	1.5	1.6×10^{-11}	310	1.1	2.4×10^{-11}
081024A	150	161.2	55–60	310	−1.5	1.5×10^{-12}	190	−2.0	2.2×10^{-12}
090102	5344	83.1	33–48	400	−0.1	8.4×10^{-12}	230	−0.3	1.8×10^{-11}
090418A	261	30.4	86–88	190	1.0	1.0×10^{-11}	120	1.7	3.0×10^{-11}
090429B	141	158.8	70–88	180	1.1	3.9×10^{-12}	120	1.0	9.6×10^{-12}
090515	356	78.8	37–57	340	0.1	6.3×10^{-12}	220	1.2	2.5×10^{-11}

Notes. Upper limits are given at the 99% confidence level in terms of νF_ν at $E_{\rm th}$, assuming the spectral indices of 2.5 and 3.5 for the standard-source and soft-source analysis, respectively, in units of erg cm^{-2} s^{-1}.

[a] Time between the GRB trigger time ($T_{\rm trig}$) and the beginning of VERITAS GRB observation.

[b] Duration of VERITAS observation.

[c] Elevation range of the VERITAS observation.

[d] The VERITAS energy threshold.

[e] Statistical significance (standard deviations) of signal counts observed by VERITAS at the GRB position.

effective area of VERITAS is multiplied by the assumed intrinsic spectrum of the burst, which we take to be $\Gamma = 2.5$. The total flux is then calculated by integrating the intrinsic differential flux of the GRB multiplied by the effective area of VERITAS, over all energies at which the product is non-negligible. This process is repeated, substituting an EBL-attenuated burst spectrum for the intrinsic burst spectrum. The ratio of the total photon flux obtained using the intrinsic burst spectrum to the total photon flux obtained using the EBL-attenuated burst spectrum gives the attenuation factor for that particular GRB observation. For the EBL-corrected upper limits obtained using the soft-source analysis, there is an extra correction factor to account for the assumed intrinsic burst spectrum ($\Gamma = 2.5$) relative to the limits obtained in Table 2 which assumes a softer observed spectrum ($\Gamma = 3.5$). The attenuation factors and redshift-corrected upper limits for GRBs with known redshift are shown in Table 3. Not surprisingly, the attenuation depends strongly on both the redshift and the energy threshold for a particular observation, but under good observing conditions, specifically at small zenith angles, reasonable sensitivity out to $z \sim 2$ is attainable with VERITAS.

The search for VHE gamma rays over timescales optimized for VERITAS sensitivity to a source with $\frac{dN}{dE} \sim t^{-1.5}$ behavior was performed as described in the previous section. Table 4 shows the results of this search. No emission associated with any GRB in the sample of 16 presented in this paper is found. The distributions of significances for both the soft and standard optimum time analyses are shown in Figure 4. For five of the

Table 3
Redshift-corrected VERITAS Upper Limits on VHE Emission from Nine *Swift*-detected GRBs

GRB	Redshift (z)	Attenuation Factor	Standard-source Analysis Upper Limit	Soft-source Analysis Upper Limit
070419A	0.97	1.5×10^{-4}	5.4×10^{-8}	2.8×10^{-8}
070521	0.553	0.2	2.1×10^{-11}	2.9×10^{-11}
071020	2.145	1.2×10^{-8}	1.5×10^{-3}	7.0×10^{-4}
080310	2.43	3.1×10^{-4}	7.0×10^{-9}	1.4×10^{-8}
080330	1.51	0.027	1.5×10^{-10}	1.2×10^{-10}
080604	1.4	4.7×10^{-3}	1.0×10^{-9}	9.9×10^{-10}
080607	3.036	1.6×10^{-7}	1.1×10^{-4}	6.8×10^{-5}
090102	1.55	7.1×10^{-5}	1.2×10^{-7}	8.1×10^{-8}
090418A	1.608	0.03	3.1×10^{-10}	6.0×10^{-10}

Notes. Upper limit and threshold energy ($E_{\rm th}$) of each GRB defined as in Table 2. The attenuation factor is explained in the text.

Table 4
A Search for VHE Emission on Timescales Optimized on VERITAS Sensitivity to a Power-law Afterglow Decay $\sim t^{-1.5}$

GRB	Duration(s)	Standard-source Analysis					Soft-source Analysis				
		$N_{\rm on}$	$N_{\rm off}$	σ[a]	$E_{\rm th}$ (GeV)	Upper Limit	$N_{\rm on}$	$N_{\rm off}$	σ[a]	$E_{\rm th}$ (GeV)	Upper Limit
070223	2.7×10^4	...	...	...	...	...	...	...	...	...	...
070419A	477	2	14	0.8	720	4.0×10^{-11}	2	42	−0.9	420	4.6×10^{-11}
070521	1809	3	113	−1.7	170	3.1×10^{-12}	23	364	−0.9	110	1.6×10^{-11}
070612B	325	3	21	0.9	470	3.8×10^{-11}	7	58	1.1	270	9.3×10^{-11}
071020	8509	...	...	...	...	...	...	...	...	...	...
080129	2356	...	...	...	...	...	...	...	...	...	...
080310	553	3	23	−0.2	480	3.2×10^{-11}	13	55	1.4	290	7.9×10^{-11}
080330	252	0	15	N/A[b]	260	2.4×10^{-11}	6	43	−0.2	170	1.4×10^{-10}
080409	1.1×10^4	...	...	...	...	...	...	...	...	...	...
080604	455	2	40	−0.6	200	1.5×10^{-11}	9	128	−0.3	140	3.6×10^{-11}
080607	298	4	16	1.1	390	9.2×10^{-11}	7	46	0.3	250	1.1×10^{-10}
081024A	242	1	7	−0.4	270	9.9×10^{-11}	4	29	0	190	1.9×10^{-10}
090102	8647	...	...	...	...	...	...	...	...	...	...
090418A	422	3	16	0.4	190	3.1×10^{-11}	8	46	0.4	120	6.9×10^{-11}
090429B	228	2	7	0.8	200	9.9×10^{-11}	4	27	0.1	140	1.5×10^{-10}
090515	576	4	24	0.3	320	2.7×10^{-11}	11	72	0.8	210	6.2×10^{-11}

Notes. Upper limits defined as in Table 2.
[a] Due to the low statistics, the calculation of the Gaussian significance by Equation (17) of Li & Ma (1983) is not valid. The ratio of Poisson means, as discussed in Cousins et al. (2008) and Zhang & Ramsden (1990), is employed instead, though it should be noted that the ratio of Poisson means method is quite conservative in situations with low statistics.
[b] In the case of zero "on" counts, the corresponding Gaussian significance is not defined.

bursts, the maximally sensitive duration of observation is greater than the length of time spent observing the burst and these bursts are omitted from this analysis. This occurred when the delay to the beginning of VERITAS observations was sufficiently long.

No significant excess of VHE gamma-ray events coincident with the large X-ray flare corresponding to the interval $T_{\rm trig}$ + 475 s to $T_{\rm trig}$ + 750 s during the afterglow of GRB 080310 (see Figure 2) is found. After accounting for gamma-ray attenuation by the EBL, the soft-source analysis returns an integral upper limit of 9.8×10^{-8} photon cm^{-2} s^{-1} above 310 GeV. Though the flare was quite bright in the XRT band, increasing by ∼3 orders of magnitude relative to the underlying afterglow, the burst was at a moderate redshift ($z = 2.4$) so the VHE gamma-ray attenuation is presumably significant.

6. DISCUSSION

The upper limits on VHE emission presented here provide strong constraints on the amount of energy released during the early-afterglow phase of GRBs. The limits themselves, however, are not sufficient to reveal much without taking into context the effects of the EBL and the intrinsic properties of each GRB. The nine bursts with measured redshifts have a mean and median redshift of 1.6 and 1.7, respectively. Assuming an EBL model (Gilmore et al. 2009), one may convert the upper limits obtained from the VERITAS observations to limits on the intrinsic GRB flux as is done in Table 3. The GRBs without measured redshifts are of less utility but, as a first approximation, one may assume a redshift of $z = 2.5$, which is the approximate median of all of GRBs with known redshift detected by *Swift* (Gehrels et al. 2009), to correct for the gamma-ray attenuation from the EBL.

After the VERITAS upper limits are corrected for EBL effects, we compare the VHE upper limits on the fluence above 200 GeV with the fluence of the GRB as measured by the *Swift*-BAT in the 15–350 keV energy range (Butler et al. 2007, 2010) that is taken as a proxy for the overall intensity of the burst. To account for the different delays and durations of the VERITAS observations, we calculate $t_{\rm med}$, the time since the beginning of the VERITAS observations of the GRB at which

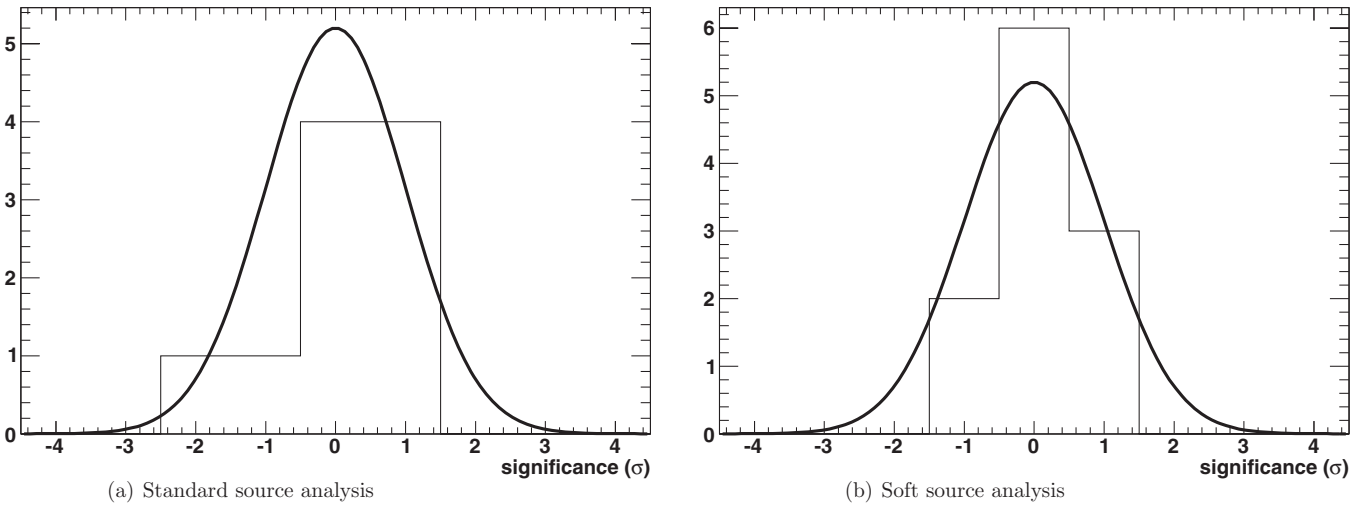

(a) Standard source analysis (b) Soft source analysis

Figure 4. Significance histograms obtained from an analysis of the GRBs in the sample over timescales for which VERITAS is maximally sensitive to a burst with a $t^{-1.5}$ power-law afterglow. Both standard- and soft-source analyses were performed. Included in the figures is the normalized Gaussian distribution of mean zero and variance one that the significance histograms should follow if no signal is present. The GRB significances are consistent with having been drawn from the aforementioned Gaussian distribution.

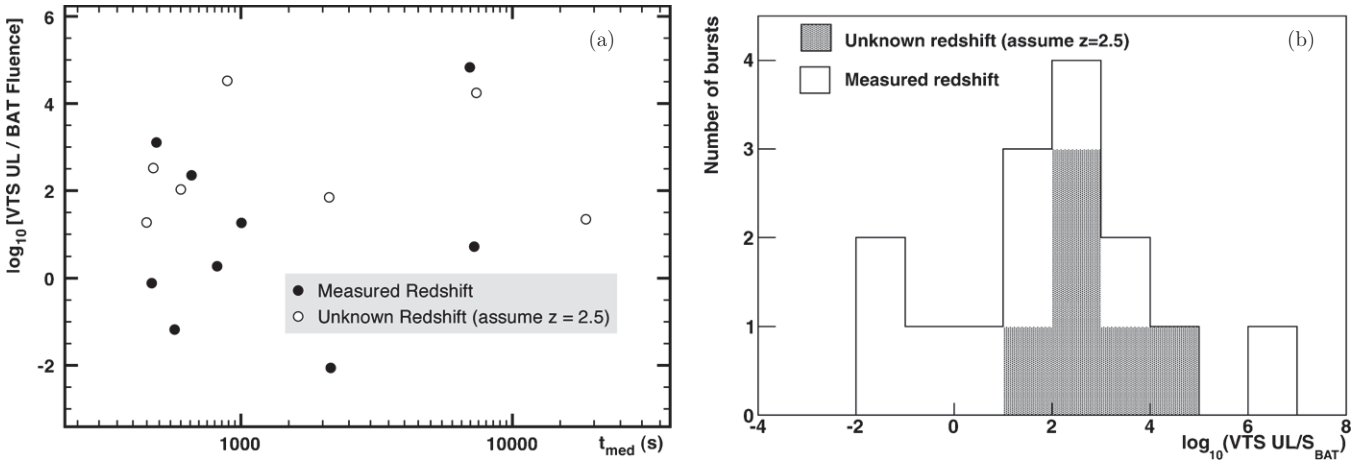

Figure 5. (a) EBL-corrected VERITAS integral fluence upper limits above 200 GeV, divided by the fluence measured by the *Swift*-BAT in the 15–350 keV energy band as a function of $t_{\rm med}$ as defined in the text. (b) A histogram of the ratio of the VERITAS integral fluence upper limit above 200 GeV, now integrated over the time period $t - T_{\rm trig} > 300$ s, to the Swift-BAT fluence. One burst, GRB 080409 is omitted in this plot as the VERITAS upper limit on the fluence of this burst is 11 orders of magnitude above the fluence measured by the BAT.

we expect to detect half of the photon signal, assuming a time profile of the GRB afterglow of $\frac{dN}{dE} \propto t^{-1.5}$ that is motivated by the high-energy afterglows observed by the *Fermi*-LAT. The ratio of VERITAS upper limit on the fluence above 200 GeV to the BAT fluence versus $t_{\rm med}$ is plotted in the left panel of Figure 5 for each burst. Since we assume a known time dependence of the VHE afterglow, we may calculate this ratio for any time period after the start of the GRB, which we take to be $t - T_{\rm trig} > 300$ s. Then for each GRB, we calculate the fractional upper limit on the VHE gamma-ray fluence over the entire afterglow ($300 < t - T_{\rm trig} < \infty$) relative to the fluence measured by the BAT. A histogram of this quantity is plotted in the right panel of Figure 5. It should be noted that if the bursts with unknown redshift are assumed to have the mean redshift of the GRBs in our sample ($z = 1.7$) as opposed to mean redshift detected by *Swift* ($z = 2.5$), then the distribution of bursts with unknown redshift moves to the left and more closely follows the distribution of known-z bursts.

These results show that for several bursts the VHE component of the GRB afterglow is less than the energy released in the *Swift*-BAT band during the prompt phase of the burst. With observation delays often on the order of a few hundred seconds, the VERITAS upper limits begin to restrict theoretical models in which the afterglow from the forward external shock contains an SSC component in addition to the synchrotron component (Xue et al. 2009).

VERITAS observations taken contemporaneously with X-ray flares during GRB afterglows are also of interest. Over the time period of the flare observed during the afterglow of GRB 080310, the VERITAS upper limits constrain the integral of F_ν above 300 GeV to be less than 9.4×10^{-8} erg cm^{-2} s^{-1}, which is a factor of $\sim$12 above the peak flux observed by the *Swift*-XRT in the 0.3–10 keV band. In light of the fact that GRB 080310 was at a redshift of nearly 2.5, it is clear that VHE observations of a strong X-ray flare from a low-redshift GRB could challenge some models in which SSC processes produce VHE emission simultaneously and with comparable intensity to the X-ray emission during the flare (Fan et al. 2008) and add detail to our understanding of the processes occurring in GRB afterglows.

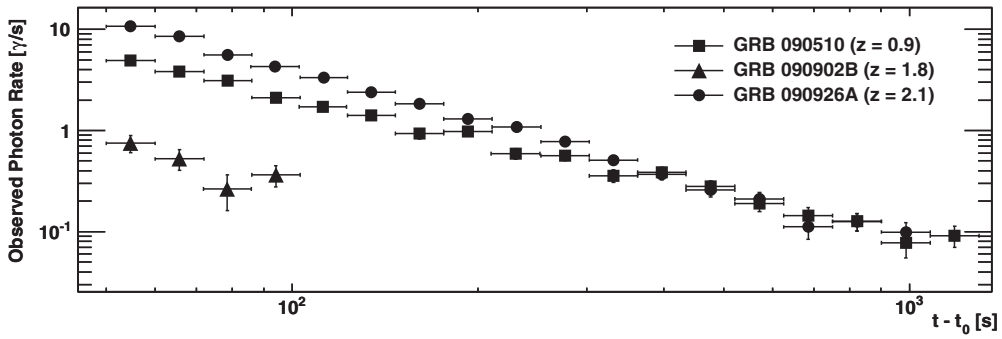

Figure 6. Predicted VERITAS light curves for three of the four brightest *Fermi*-LAT GRBs. The fourth, GRB 080916C had a redshift of nearly 4.4 and VHE emission is predicted to be too attenuated by the EBL to be detectable by VERITAS. The EBL model of Gilmore et al. (2009) is used to estimate the attenuation of the VHE γ-rays. The elevation of the burst with respect to VERITAS is chosen to be 70° and no intrinsic spectral cutoff of the high-energy emission is assumed. Each point signifies a detection of at least three standard deviations (σ) in that time bin.

7. FUTURE PROSPECTS

The detection of VHE emission from GRBs in light of recent observations by the *Fermi* and *Swift* space telescopes remains a challenging, though not unreasonable, prospect. The number of GRBs found by the LAT to emit GeV radiation is small, with a detection rate on the order of one every few months. Combined with the ∼10%–15% duty cycle of an IACT array such as VERITAS, the probability of simultaneous observation of such bursts is not high. On the other hand, >30 GeV emission has been detected from both short (Abdo et al. 2009a) and long (Abdo et al. 2009b) GRBs and, in the latter case, persists well after the prompt phase of the burst. Furthermore, these observations indicate that the high-energy photon absorption due to the EBL is not so severe (Abdo et al. 2010) as to rule out ground-based VHE detections that in turn could strongly constrain models of GRB physics (Cenko et al. 2011), as well as those of the EBL.

Approximately one of every fifteen GRBs detected by the *Fermi*-GBM is detected by the LAT (provided the burst also falls in the LAT FOV). Though they are rare, some luminous, LAT-detected GRBs should be detectable by VERITAS. Taking the spectral and temporal characteristics of the high-energy emission from the four brightest *Fermi*-LAT bursts: GRB 080916C (Abdo et al. 2009c), GRB 090510 (Pasquale et al. 2010), GRB 090902B (Abdo et al. 2009b), and GRB 090926A (Ackermann et al. 2011), we estimate the expected flux of VHE photons in the energy range of VERITAS as a function of time. Figure 6 shows the light curves of three of these four bursts that we predict to have been detectable by VERITAS. GRB 090510 and GRB 090926A produce significant signal in the VERITAS band for roughly a thousand seconds. GRB 080916C had a redshift of $z > 4$ and the VHE emission is extremely suppressed through interaction with the EBL. It is observed that even for bursts with redshift between 1 and 2, some exceptional GRBs may be quite bright in the VERITAS energy band. However, in the absence of delayed activity (e.g., that associated with X-ray flares) the power-law temporal decay of the late-time, high-energy emission necessitates relatively rapid follow-up observations. VERITAS has made several GRB follow-up observations with delays of less than 100 s and has a median response time of 328 s[31] and therefore may be capable of detecting the same high-energy component that the *Fermi*-LAT detects, provided it extends to >100 GeV energies.

[31] These numbers are based on all GRBs observed by VERITAS from 2007 January through 2009 June, including *Fermi*-GBM triggered observations that are not included in this paper.

VERITAS continues to take follow-up observations of GRBs. In the summer of 2009, one of the telescopes in the VERITAS array was moved to a new position that resulted in an improvement in sensitivity of ∼30%. By fall 2012, an upgrade of the telescope-level trigger system and the replacement of existing PMTs with a more sensitive PMT will significantly increase the low-energy response of the instrument. This is particularly important for GRB observations as the EBL significantly attenuates the high-energy component of sources with appreciable redshifts. Additionally, work is ongoing to improve the sensitivity of the array with respect to low elevation targets, which make up the majority of GRB observations. Response times for immediately observable bursts have been gradually decreasing and efforts are underway to increase the slewing speed of the telescope motors to reduce these times further. Such efforts are increasing the GRB science capability of VERITAS and will lead to a more thorough characterization of the highest energy emission from GRBs.

8. CONCLUSIONS

The VERITAS telescope array was used to make follow-up observations of 29 satellite-detected GRBs during the period of 2007 January through 2009 June. Due to the incorporation of real-time alerts from the GCN into the VERITAS pointing and control software, relatively small observation delays (down to 91 s) were achieved. After quality selection cuts, data from 16 of the 29 bursts were analyzed and those results are presented here. No significant excess of VHE gamma rays from any of the bursts is detected and the 99% confidence level upper limits on the photon flux are derived. Assuming a $t^{-1.5}$ temporal decay of the VHE afterglow, limits on the VHE afterglow fluence relative to the prompt fluence detected by the *Swift*-BAT are calculated. For more than half of the GRBs with known redshift in our sample, the VHE afterglow fluence is constrained to be less than the prompt, low-energy gamma-ray fluence.

In the context of recent GRB observations by *Fermi*-LAT, prospects for detection of VHE emission by VERITAS are good, assuming the most straightforward extrapolation of the spectral and temporal characteristics of the high-energy emission. Contemporaneous early-afterglow observations of a GRB by the *Fermi*-LAT and an IACT array would provide valuable insights into understanding the physical processes at work in the GRB environment as well as constrain the properties of the EBL.

This research is supported by grants from the US Department of Energy, the US National Science Foundation, and the

Smithsonian Institution, by NSERC in Canada, by Science Foundation Ireland (SFI 10/RFP/AST2748), and by STFC in the UK. We acknowledge the excellent work of the technical support staff at the FLWO and the collaborating institutions in the construction and operation of the instrument. We acknowledge the support provided by NASA *Swift* Guest Investigator (GI) grant NNX09AR06G. T. Aune gratefully acknowledges the support provided by a NASA Graduate Student Researchers Program fellowship. This work made use of data supplied by the UK Swift Science Data Centre at the University of Leicester.

Facility: VERITAS

REFERENCES

Abdo, A. A., Ackermann, M., Ajello, M., et al. 2009a, Nature, 462, 331
Abdo, A. A., Ackermann, M., Ajello, M., et al. 2009b, ApJ, 706, L138
Abdo, A. A., Ackermann, M., Ajello, M., et al. 2010, ApJ, 723, 1082
Abdo, A. A., Ackermann, M., Ajello, M., et al. 2011, ApJ, 734, L27
Abdo, A. A., Ackermann, M., Arimoto, M., et al. 2009c, Science, 323, 1688
Ackermann, M., Ajello, M., Asano, K., et al. 2011, ApJ, 729, 114
Aharonian, F., Akhperjanian, A. G., Barres de Almeida, U., et al. 2009, A&A, 495, 505
Aharonian, F., Akhperjanian, A., Barrio, J., et al. 2001, A&A, 370, 112
Albert, J., Aliu, E., Anderhub, H., et al. 2007, ApJ, 667, 358
Atkins, R., Benbow, W., Berley, D., et al. 2000, ApJ, 533, L119
Atwood, W. B., Abdo, A. A., Ackermann, M., et al. 2009, ApJ, 697, 1071
Beloborodov, A. M. 2005, ApJ, 618, L13
Berge, D., Funk, S., & Hinton, J. 2007, A&A, 466, 1219
Bottcher, M., & Dermer, C. D. 1998, ApJ, 499, L131
Burrows, D. N., Romano, P., Falcone, A., et al. 2005, Science, 309, 1833
Butler, N. R., Bloom, J. S., & Poznanski, D. 2010, ApJ, 711, 495
Butler, N. R., Kocevski, D., Bloom, J. S., & Curtis, J. L. 2007, ApJ, 671, 656
Cenko, S. B., Frail, D. A., Harrison, F. A., et al. 2011, ApJ, 732, 29
Cenko, S. B., Gezari, S., Small, T., Fox, D. B., & Chornock, R. 2007, GRB Coordinates Network, 6322, 1
Chincarini, G., Moretti, A., Romano, P., et al. 2007, ApJ, 671, 1903
Chornock, R., Cenko, S. B., Griffith, C. V., et al. 2009, GRB Coordinates Network, 9151, 1
Cogan, P. 2008, in Proc. 30th Int. Cosmic Ray Conf., Vol. 3, Mérida, México, ed. R. Caballero et al. (Mexico: Universidad Nacional Autónoma de México), 1385
Connaughton, V., Akerlof, C. W., Barthelmy, S., et al. 1997, ApJ, 479, 859
Cousins, R., Linnemann, J., & Tucker, J. 2008, Nucl. Instrum. Methods Phys. Res. A, 595, 480
Dermer, C. D. 2007, ApJ, 664, 384
Dermer, C. D., Chiang, J., & Mitman, K. E. 2000, ApJ, 537, 785
de Ugarte Postigo, A., Jakobsson, P., Malesani, D., et al. 2009, GRB Coordinates Network, 8766, 1
Evans, P. A., Beardmore, A. P., Page, K. L., et al. 2007, A&A, 469, 379
Evans, P. A., Beardmore, A. P., Page, K. L., et al. 2009, MNRAS, 397, 1177
Falcone, A. D., Morris, D., Racusin, J., et al. 2007, ApJ, 671, 1921
Fan, Y., Piran, T., Narayan, R., & Wei, D. 2008, MNRAS, 384, 1483
Galli, A., & Piro, L. 2008, A&A, 489, 1073
Gehrels, N., Ramirez-Ruiz, E., & Fox, D. B. 2009, ARA&A, 47, 567
Ghisellini, G., Ghirlanda, G., Nava, L., & Celotti, A. 2010, MNRAS, 403, 926
Gilmore, R. C., Madau, P., Primack, J. R., et al. 2009, MNRAS, 399, 1694
Hattori, T., Aoki, K., & Kawai, N. 2007, GRB Coordinates Network, 6444, 1
Hillas, A. M. 1985, in Proc. XIX Int. Cosmic Ray Conf., Vol. 3, La Jolla, California, U.S.A., ed. F. C. Jones (Washington, DC: NASA), 445
Holder, J., Atkins, R. W., Badran, H. M., et al. 2006, Astropart. Phys., 25, 391
Jakobsson, P., Vreeswijk, P. M., Hjorth, J., et al. 2007, GRB Coordinates Network, 6952, 1
Kaneko, Y., Preece, R. D., Briggs, M. S., et al. 2006, ApJS, 166, 298
Klebesadel, R. W., Strong, I. B., & Olson, R. A. 1973, ApJ, 182, L85
Krawczynski, H., Carter-Lewis, D. A., Duke, C., et al. 2006, Astropart. Phys., 25, 380
Kumar, P., & Barniol Duran, R. 2009, MNRAS, 400, L75
Li, T., & Ma, Y. 1983, ApJ, 272, 317
Malesani, D., Fynbo, J. P. U., Jakobsson, P., Vreeswijk, P. M., & Niemi, S.-M. 2008, GRB Coordinates Network, 7544, 1
Meszaros, P., & Rees, M. J. 1994, MNRAS, 269, L41
Murase, K., Ioka, K., Nagataki, S., & Nakamura, T. 2008, Phys. Rev. D, 78, 023005
Panaitescu, A. 2008, MNRAS, 385, 1628
Pasquale, M. D., Schady, P., Kuin, N. P. M., et al. 2010, ApJ, 709, L146
Pe'er, A., & Waxman, E. 2005, ApJ, 633, 1018
Perkins, J. S., Maier, G., & The VERITAS Collaboration 2009, Proc. 2009 Fermi Symp., Washington, D.C., eConf C091122 (arXiv:0912.3841)
Piran, T. 1999, Phys. Rep., 314, 575
Prochaska, J. X., Murphy, M., Malec, A. L., & Miller, K. 2008a, GRB Coordinates Network, 7388, 1
Prochaska, J. X., Shiode, J., Bloom, J. S., et al. 2008b, GRB Coordinates Network, 7849, 1
Rolke, W. A., López, A. M., & Conrad, J. 2005, Nucl. Instrum. Methods Phys. Res. A, 551, 493
Wang, X. Y., Dai, Z. G., & Lu, T. 2001, ApJ, 556, 1010
Wang, X., Li, Z., & Mészáros, P. 2006, ApJ, 641, L89
Waxman, E. 2004, ApJ, 606, 988
Wiersema, K., Graham, J., Tanvir, N., et al. 2008, GRB Coordinates Network, 7818, 1
Xue, R. R., Tam, P. H., Wagner, S. J., et al. 2009, ApJ, 703, 60
Zhang, B., & Mészáros, P. 2001, ApJ, 559, 110
Zhang, S. N., & Ramsden, D. 1990, Exp. Astron., 1, 145
Zou, Y., Fan, Y., & Piran, T. 2009, MNRAS, 396, 1163